Click Here for Full Article

Variations in the chorus source location deduced from fluctuations of the ambient magnetic field: Comparison of Cluster data and the backward wave oscillator model

B. V. Kozelov,[1,2] A. G. Demekhov,[3] E. E. Titova,[2] V. Y. Trakhtengerts,[3,4] O. Santolik,[5,6] E. Macusova,[6] D. A. Gurnett,[7] and J. S. Pickett[7]

Received 16 October 2007; revised 14 March 2008; accepted 15 April 2008; published 18 June 2008.

[1] We study the motion of the source region of magnetospheric chorus emissions using multipoint measurements of VLF wave emissions and geomagnetic field onboard the Cluster spacecraft. The geomagnetic field data are matched to a parameterized model of the local magnetic field, and the spatiotemporal dynamics of the magnetic field are obtained on this basis. The wave data from the Wide Band Data instrument are used to obtain the power spectral density and number of chorus elements. Comparison of these data shows that the chorus remains related to the magnetic field minimum, while the position of this minimum can vary rather strongly during periods of enhanced geomagnetic activity. These results support the backward wave oscillator (BWO) model of chorus emissions, which attributes chorus generation to an absolute instability of whistler mode waves in the presence of a step-like velocity distribution of energetic electrons. Such an instability takes place in a small vicinity of the local "magnetic equator" of a magnetic field line. Quantitative agreement between the data and the model is demonstrated by variation of the statistical chorus characteristics with changing of the deduced BWO parameters.

Citation: Kozelov, B. V., A. G. Demekhov, E. E. Titova, V. Y. Trakhtengerts, O. Santolik, E. Macusova, D. A. Gurnett, and J. S. Pickett (2008), Variations in the chorus source location deduced from fluctuations of the ambient magnetic field: Comparison of Cluster data and the backward wave oscillator model, *J. Geophys. Res.*, *113*, A06216, doi:10.1029/2007JA012886.

1. Introduction

[2] Recently the multipoint measurements onboard the Cluster spacecraft gave new possibilities to study VLF wave emissions [*Gurnett et al.*, 2001]. The "chorus" emissions are clearly distinguishable because of their discrete nature and therefore it is possible to follow the location of their generation region. Using the high time resolution Wide Band Data (WBD) instrument measurements it was shown that the size of the chorus generation region is of the order of a few hundreds of kilometers perpendicular to the magnetic field line direction [*Santolik and Gurnett*, 2003]. The wave data from the Spatio-Temporal Analysis Field Fluctuation (STAFF) instrument was used to obtain the energy flux in chorus waves, and the chorus source region is found as the region where the energy flux is bidirectional. The region of VLF chorus generation was shown to be located near the geomagnetic equator [*LeDocq et al.*, 1998; *Santolik et al.*, 2004] and be extremely variable in space and time [*Santolik et al.*, 2004, 2005].

[3] According to the backward wave oscillator (BWO) model of chorus generation [*Trakhtengerts*, 1999; *Trakhtengerts et al.*, 2004], the parameters of the chorus source region strongly depend on the magnetic field inhomogeneity. To date, theoretical estimates and their comparison with data were based on the idealized magnetic field model in the equatorial plane of the magnetosphere. Taking into account the sensitivity of this region to the magnetospheric disturbances, the instant BWO parameters should also vary with respect to their averaged values. In this paper, we try to answer the following questions: (1) Can we obtain the local BWO geometry directly from satellite data and (2) can we describe the dynamics of the BWO geometry during events of interest?

[4] As the main characteristics of the magnetospheric BWO we consider its position on the magnetic field line (position of the minimum of the field strength $\mathbf{B}_{\min}$ measured along the magnetic field line) and the effective length along the magnetic field line (L_{BWO}). To estimate these quantities we need to know the magnetic field strength along the magnetic field line at each time moment. We can deduce the local magnetic field configuration from Cluster observations, but the satellites give us values of the magnetic field in

[1]Department of Physics and Technology, University of Tromsø, Tromsø, Norway.
[2]Polar Geophysical Institute, Apatity, Russia.
[3]Institute of Applied Physics, Nizhny Novgorod, Russia.
[4]Deceased 4 December 2007.
[5]Institute of Atmospheric Physics, Prague, Czech Republic.
[6]Department of Mathematics and Physics, Charles University, Prague, Czech Republic.
[7]Department of Physics and Astronomy, University of Iowa, Iowa City, Iowa, USA.

Copyright 2008 by the American Geophysical Union.
0148-0227/08/2007JA012886$09.00

four points only. Therefore, a magnetospheric model is needed. However, the known global magnetospheric models are statistical, and, therefore, they cannot describe the specific dynamics of observed events. Here we will use a dynamical model of local magnetic field constructed from the statistical Tsyganenko model and additional currents to fit evolution of the ambient geomagnetic field measured by the onboard fluxgate magnetometers [*Balogh et al.*, 2001]. Previously, a similar approach but with one additional current was used to describe dynamics of the magnetic field in the night sector at 4–10 R_E during a substorm event observed by the CRRES satellite [*Kozelov and Kozelova*, 2003a]. Here we use a more complex model with two additional currents.

2. Dynamical Magnetic Field Model

[5] The dynamical magnetic field model has been constructed on the basis of the statistical magnetospheric models given by *Tsyganenko and Stern* [1996] and *Tsyganenko and Sitnov* [2005]. We have then compared the output of this model to the magnetic field measured onboard the Cluster spacecraft by the Fluxgate Magnetometer (FGM) instruments [*Balogh et al.*, 2001]. Unfortunately, the deviations of the Tsyganenko 2004 model [*Tsyganenko and Sitnov*, 2005] from the locally observed values during the events of interest were too large. Therefore, we use Tsy96 model [*Tsyganenko and Stern*, 1996] with parameters adjusted to minimize the deviations from the local observations. The deviation of the observed magnetic field from the value modeled by the Tsy96 model is

$$\Delta\mathbf{B} = \mathbf{B}_{\text{observed}} - \mathbf{B}_{\text{Tsy96}}. \tag{1}$$

[6] The region of interest for us is located in the nightside magnetosphere at 4–5 R_E near the equatorial plane in the solar-magnetic (SM) frame. The magnetic field configuration in this region is determined by the Earth's magnetic field (mainly magnetic dipole) and magnetic field of external sources: the ring current, the earthward part of cross-tail current, etc. [*Tsyganenko and Stern*, 1996]. Average contributions of all these sources are included in the statistical Tsy96 model. For the time intervals of several minutes the internal magnetic field of the Earth and the contribution of the ring current can be assumed constant; therefore, the temporal variations observed in the region of interest should be a result of the plasma sheet variations. Variations in the particle fluxes during magnetospheric disturbances lead to the variations in the magnetic field which we associate with the magnetic field deviation according to equation (1). To produce this deviation we supplement the model with two additional linear currents located far enough from the region of interest. We assume that each current is located in the plane parallel to the magnetic equator and the parameters of the currents are adjusted to yield the deviations of the magnetic field observed by a pair of the Cluster satellites from the values modeled by the Tsy96 model. This pair is selected between the four spacecraft. The reason why we use only two selected spacecraft is that the two linear currents become fully determined by the data of two spacecraft.

[7] These additional currents may be interpreted as effective "skin currents" at the boundaries of the plasma sheet during magnetospheric disturbances. The region of interest is located inside the region limited by these currents in the z direction.

[8] The additional currents included in the model lead to smooth deformation of the statistical magnetic field lines in the region of interest. This deformation ensures a good correspondence of the model field to the measured one in at least two points occupied by Cluster satellites. Therefore, our model gives a better approximation of the local magnetic field than the statistical model, but still may have significant uncertainty at a large distance from the satellite position. We checked the stability of our model with respect to the qualitative conclusions by varying its fixed parameters, such as the distance between the additional current sheets and the pair of spacecraft used for fitting.

[9] For the positions of two Cluster satellites, the magnetic field induced in vacuum by two currents is given by Ampere's law

$$\Delta\mathbf{B}_{1,2} = \frac{\mu_0}{2\pi}\left(\frac{I_1\left[\mathbf{i}_1 \times \left(\mathbf{p}_{1,2} - \mathbf{r}_1\right)\right]}{\left|\mathbf{i}_1 \times \left(\mathbf{p}_{1,2} - \mathbf{r}_1\right)\right|^2} + \frac{I_2\left[\mathbf{i}_2 \times \left(\mathbf{p}_{1,2} - \mathbf{r}_2\right)\right]}{\left|\mathbf{i}_2 \times \left(\mathbf{p}_{1,2} - \mathbf{r}_2\right)\right|^2}\right), \tag{2}$$

where $\mathbf{p}_{1,2}$ are known positions of two Cluster satellites, I_1 and I_2 are two line currents, $\mathbf{i}_1$ and $\mathbf{i}_2$ are unit vectors along their directions, $\mathbf{r}_1$ and $\mathbf{r}_2$ are points at the line currents. To reduce the number of variables we suppose that the two line currents are localized in two planes perpendicular to the z axis of the SM coordinates, $r_{1z} = z_1$, $r_{2z} = z_2$, $i_{1z} = 0$, $i_{2z} = 0$. Here i_{1y} and i_{2y} are linked to i_{1x} and i_{2x} since $\mathbf{i}_1$ and $\mathbf{i}_2$ are unit vectors. Since $\mathbf{r}_1$ and $\mathbf{r}_2$ are arbitrary points at the line currents, we can define

$$\frac{r_{1y}}{r_{1x}} = \frac{r_{2y}}{r_{2x}} = \frac{p_{1y} + p_{2y}}{p_{1x} + p_{2x}}. \tag{3}$$

Thus, we have only six scalar variables (I_1, I_2, r_{1x}, r_{2x}, i_{1x}, and i_{2x}) in six equations. The system of six equations has been analytically simplified in SM coordinates to a system of two equations. The latter system was solved numerically for each time moment. More details about the model equations are presented in the Appendix A.

[10] A new field line has been traced from the position of the satellite with the inclusion of the two new currents at each time step. Then, the position of $|\mathbf{B}_{\min}|$ on a magnetic field line gives us the central position of the local BWO. According to *Trakhtengerts* [1995] and *Demekhov et al.* [2003], the effective length of the local BWO can be estimated as the distance $L_{\text{BWO}} = l_2 - l_1$ between two points satisfying the following relations

$$|\Delta\varphi| = \left|\int \Delta \frac{dz}{v_\parallel}\right| = \frac{\omega_{\text{HL}}}{v_\parallel}\int_{l_1}^{l_2} b(l)dl = \pi, \tag{4}$$

where $\Delta = \omega - \omega_H(l) - k_\parallel v_\parallel$ is the frequency mismatch from the cyclotron resonance, $\omega_H = \omega_{\text{HL}}(1 + b(l))$ is the electron gyrofrequency, the subscript "L" denotes the values at the central position of the local BWO where $\mathbf{B} = \mathbf{B}_{\min}$, $b(l) = |\mathbf{B}(l)|/|\mathbf{B}_{\min}| - 1$, $b(l_1) = b(l_2)$. The parallel velocity $v_\parallel$ is obtained from assumption that $\Delta = 0$ in the BWO central

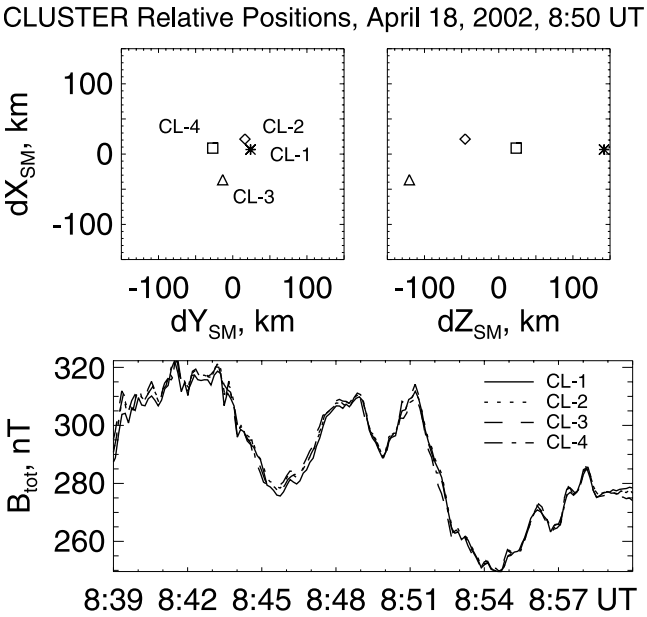

Figure 1. (top) Cluster relative positions on 18 April 2002; (bottom) observed total magnetic field along the satellites trajectories.

position where the parallel wave number $k_{||}$ is calculated from the whistler mode dispersion relation for $\omega_H = \omega_{HL}$.

3. Event on 18 April 2002

[11] Figure 1 shows the relative positions of the four Cluster satellites and the ambient magnetic field observed on 18 April 2002 near the magnetic equator. The spacecraft are closely separated; therefore the differences between the magnetic field values observed by the satellites are not large. To fit the magnetic field configuration we use the data from Cluster 1 and Cluster 3. This is the most separated pair (by ~250 km along the z coordinate and by <50 km along the x and y coordinates in the SM coordinate system). The additional currents are assumed to be at $z_1 = -1\ R_E$ and $z_2 = 1\ R_E$ ($R_E = 6370$ km is the Earth radius).

[12] The results of the modeling are presented in Figure 2 in comparison with measurements of Cluster 1. In contrast with the Tsy96 model, the dynamical model gives a perfect fit to the observed values of the magnetic field in the near-equatorial region. The observed and fitted values are so close that they are not resolved within the line thickness on the plot. Because of the close spacecraft separation, the modeled values are also close to the ones measured at the positions of the Cluster 2 and Cluster 4 spacecraft, not used in this fit. The deviation is smaller than 2 nT (<1%) for all satellites. One can see that the model gives a good fit of the magnetic field in the region near the spacecraft. The magnetic field strength along the magnetic field line crossing Cluster 1 is shown in the second panel of Figure 2. One can see a variation of the "cavity" of smaller field near the equatorial region. The center of the cavity gives us the position of the local BWO plotted on the third panel. The effective BWO length has been calculated as the distance between two points satisfying the relation (4) as shown on the fourth panel.

[13] One can see in the third and fourth panels of Figure 2 that both parameters exhibit random fluctuations; however the smoothed values have well-defined variations. These variations are the same for both satellites used in the model fitting; therefore, the plots for Cluster 3 are not shown. The BWO position varies by ±1500 km near the magnetic equatorial plane, and the effective BWO length fluctuates in the range from 3000 to 5000 km. We should note that several different positions of the additional currents have been tested for the magnetic field fitting. The resulting variations of the local BWO parameters depend very weakly on z_1 and z_2 in the range from 0.3 to 1.0 R_E. The largest dependence was found on the satellite pair used for the fitting, which can be explained by the small separation between the satellites along the z axis causing the sensitivity of the model fitting to the noise in magnetic field measurements.

[14] Because of the small distance between satellites (less than 100 km), which is smaller than the characteristic source size in the direction perpendicular to the magnetic field lines [*Santolik and Gurnett*, 2003], we can use averaging to decrease random fluctuations. Figure 3 shows the evolution of the magnetospheric BWO parameters averaged over values obtained for Cluster 1, 2, and 3 by model fitting the two pairs most separated in the z direction. For comparison, the center of the chorus source previously obtained from the VLF STAFF data [*Santolik et al.*, 2005, Figure 6] is shown in the same plot by the short dashed line. We note that the analysis of VLF STAFF data is prone to similar errors as discussed above for the magnetic field model because of the small separation between the satellites. Therefore we cannot expect one-to-one correspondence for all excursions of the minimum B position and the center of the chorus source obtained from the STAFF VLF data. However, general features (preferable position with respect to the equatorial plane, the range of variation) are similar. The most important result here is that the variation of the minimum B position along the field line agrees in general with the variation of the center of the chorus source previously obtained from the VLF STAFF data (see more detailed discussion in section 5). Thus, we obtained an observational confirmation that the chorus source remains centered near the local B minimum.

4. Event on 31 March 2001

[15] On 31 March 2001 the Cluster spacecraft were at relatively large separations, see Figure 4. There were very disturbed conditions, when the *Kp* index reached the value of 9− and *Dst* decreased to −358 nT [*Baker et al.*, 2002]. To fit the magnetic field configuration we use the data from Cluster 1 and Cluster 2 separated in the SM coordinate system by ~1200 km along the z coordinate and by ~50 km along the x and y coordinates. The results for Cluster 1 are presented in Figure 5. The results for Cluster 2 are not shown, because they look very similar. The dynamical model describes the observed values of the magnetic field sufficiently well. The deviation of the modeled values relative to the measured ones is smaller than 2 nT for the main time interval of interest (from 0705 to 0712 UT) when

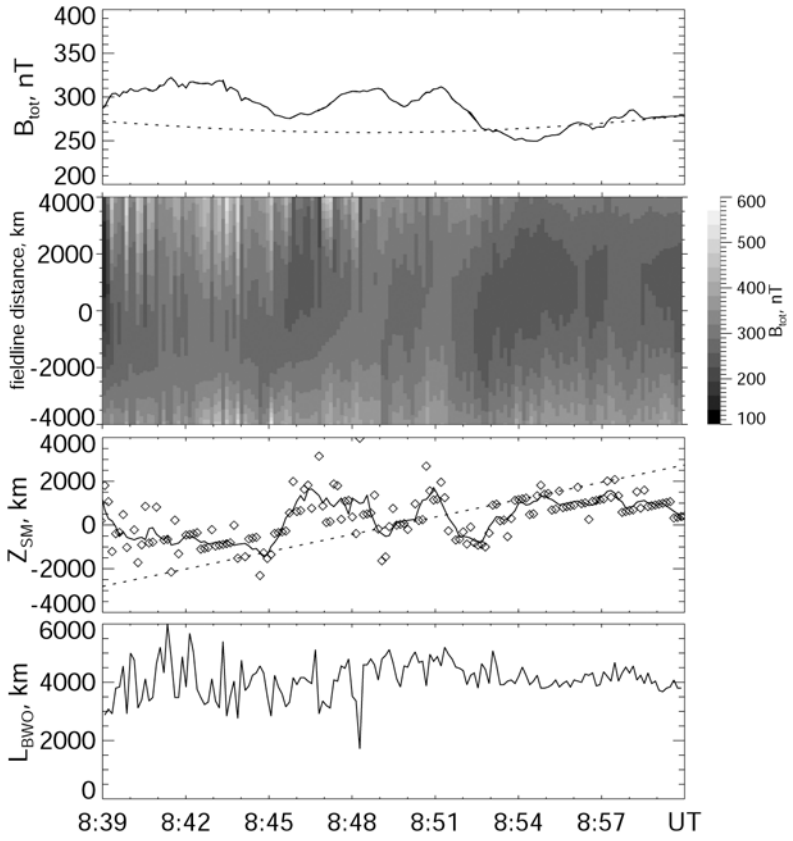

Figure 2. Results of modeling of the magnetospheric BWO configurations on 18 April 2002 for a magnetic field line at the Cluster 1 position. (first panel) Thin line (hidden by the solid line) is the observed strength of the magnetic field, dashed line is the observed strength of the magnetic field calculated by Tsy96, and solid line is the observed strength of the magnetic field fitted by a model with two additional currents. (second panel) The modeled magnetic field along the magnetic field line. (third panel) Symbols mark the calculated positions of the magnetic field minimum, and solid and dashed lines show the smoothed evolution of this position and the Cluster orbit, respectively. (fourth panel) Evolution of the estimated length of the magnetospheric BWO.

the spacecraft were near the equatorial region. Only a few times we can note a large difference between the observed and fitted values, but those cases occurred beyond the main time interval of interest. The quality of the model fitting is supported by Figure 6 which presents a comparison of the observed and modeled magnetic field for the Cluster 3 position. One can see that the model describes the magnetic field variation very well, but slightly (~5–7%) underestimates the absolute values. The Cluster 4 was located sufficiently in the perpendicular direction from Cluster 1–Cluster 2 pair, therefore it was not considered here.

[16] The parameters of the magnetospheric BWO estimated from the derived magnetic field model are presented in the third and fourth panels of Figure 5. The BWO position varies from $z_{sm} = -1000$ km to $z_{sm} = 1500$ km near the magnetic-equatorial plane; and the effective BWO length tends to decrease from ~3000 to ~2000 km during the event. The smaller values of L_{BWO} compared with the case of 18 April 2002 correspond to higher magnetic activity and a more stretched magnetic field profile.

[17] Comparison of the minimum B position obtained from local magnetic field modeling with the center of the chorus source obtained from the VLF STAFF data [*Santolik et al.*, 2005, Figure 3] is presented in Figure 7. The variation in the parallel component of the Poynting vector normalized by its standard deviation [from *Santolik et al.*, 2005, Figure 2] is also shown for Cluster 1. In this case, as well as in the case presented above, the obtained variation of the position of minimum B along the field line qualitatively agrees well with the variation of the chorus source location previously obtained from the STAFF data [*Santolik et al.*, 2005].

5. Discussion

[18] Let us first compare the technique used here with that employed previously. *Santolik et al.* [2005] estimated the variation of the central region of the VLF wave generation using the STAFF data, and they obtained the local direction of the ambient magnetic field from the FGM data. In their interpretation of the observed central positions of the source region, *Santolik et al.* [2005, Figure 8] did not attempt to model possible variations of the magnetic field strength along the individual field lines. Their interpretation was only based on the magnetic field directions observed along the spacecraft trajectories. They concluded that flapping of the global tail-like magnetic field configuration did not

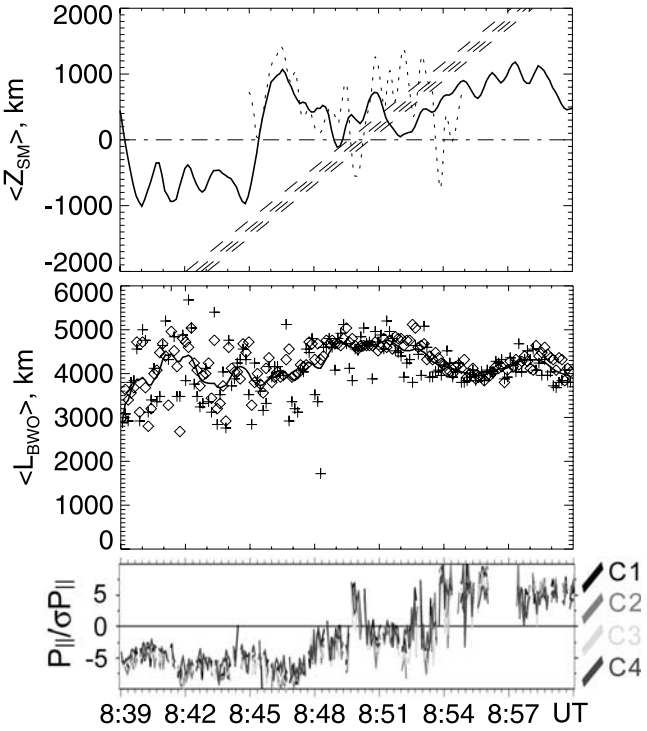

Figure 3. Parameters of the magnetospheric BWO estimated from the dynamical model of the local magnetic field. (top) Solid line is the position of the BWO center (minimum B point), short dashed line is the position of the VLF source from *Santolik et al.* [2005], and long dashed lines are the satellite trajectories. (middle) Solid line is the average values of the BWO length and symbols are the values estimated from pairs Cluster 1-Cluster 2 (diamonds) and Cluster 1-Cluster 3 (pluses). (bottom) Parallel component of the Poynting vector normalized by its standard deviation [*Santolik et al.*, 2005].

occur and that the changes in the central position of the source region are associated with the source mechanism of the chorus emissions.

[19] The method presented here employs a more refined technique for using the ambient magnetic field data in connection with the BWO theory of the chorus source mechanism. The data from two satellites are processed to construct the dynamical model of the ambient magnetic field in the local region near the spacecraft position. This model should agree well with the observed magnetic field at least at the positions of these two satellites. However, the model describes also the magnetic field at the positions of adjacent satellites even for the very disturbed case of 31 March 2001, as one can see in Figure 6. Formally, there is no restriction on the values used in equations (1)–(3) to resolve them, except the obvious condition of nonsingularity which means that the satellites should be far enough from one another and from additional currents introduced in the model. However, there are some physical reasons for selection of the satellite pair for the model fitting, since there are qualitative differences between the directions along and across (perpendicular) to the magnetic field in the considered region of the magnetosphere. As we noted in section 2, the variation of the magnetic field observed in the region of interest is probably a result of the plasma sheet variations. The spatial variations in the direction perpendicular to the magnetic field have a characteristic scale of ~100 km, which is the scale of proton gyroradius. Therefore to describe temporal variation of the selected magnetic field line we should minimize the influence of regions separated in the perpendicular direction by a larger distance than this characteristic scale. However, the shape of magnetic field lines beyond the equatorial region is mainly controlled by the internal magnetic field of the Earth and the ring current, the characteristic scale ~1000s km. Therefore the optimal field-aligned distance between the satellites should be several hundreds of kilometers. The small separation of the satellites along the magnetic field line in the case of 18 April 2002 leads to relatively large random fluctuations of the estimated BWO parameters. In this case, it is possible to decrease the random fluctuations by averaging over the values obtained for different satellites, because the small separation in the direction perpendicular to the magnetic field line guarantees that all satellites were located on the magnetic field lines which are projected in the same generation region.

[20] For the two events analyzed it was shown that the variation in the minimum B position along the field line qualitatively agrees with the variation in the center of the chorus source obtained previously from the STAFF VLF data. Thus, we have confirmed that the chorus source remains centered near the local B minimum even if the position of this minimum is shifted rather strongly from the dipole geomagnetic equator because of magnetic disturbances. These results agree well with predictions of the magnetospheric BWO model [*Trakhtengerts*, 1999; *Trakhtengerts et al.*, 2004]. Figure 8 presents results of simulations of nonlinear equations for the magnetospheric BWO [*Demekhov and Trakhtengerts*, 2005] with two magnetic field profiles corresponding to different time intervals of 18 April 2002. The plots demonstrate that the center of the chorus source region in the simulations remains near the local minimum of the geomagnetic field.

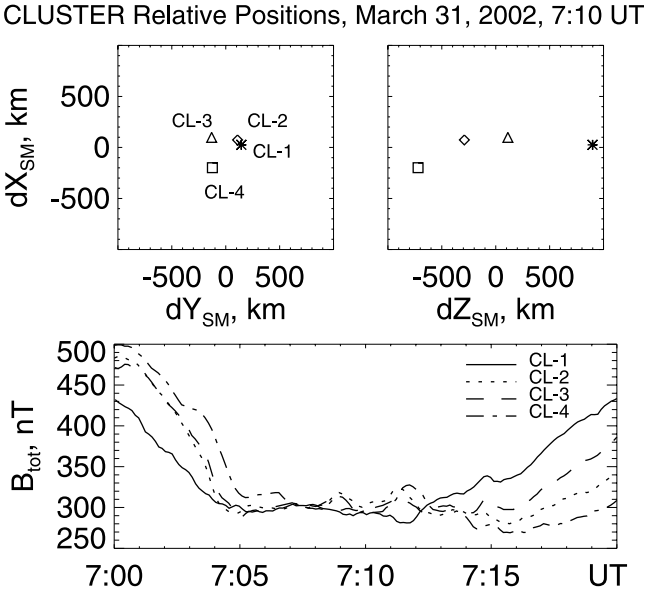

Figure 4. (top) Cluster relative positions on 31 March 2001; (bottom) observed total magnetic field along the satellites trajectories.

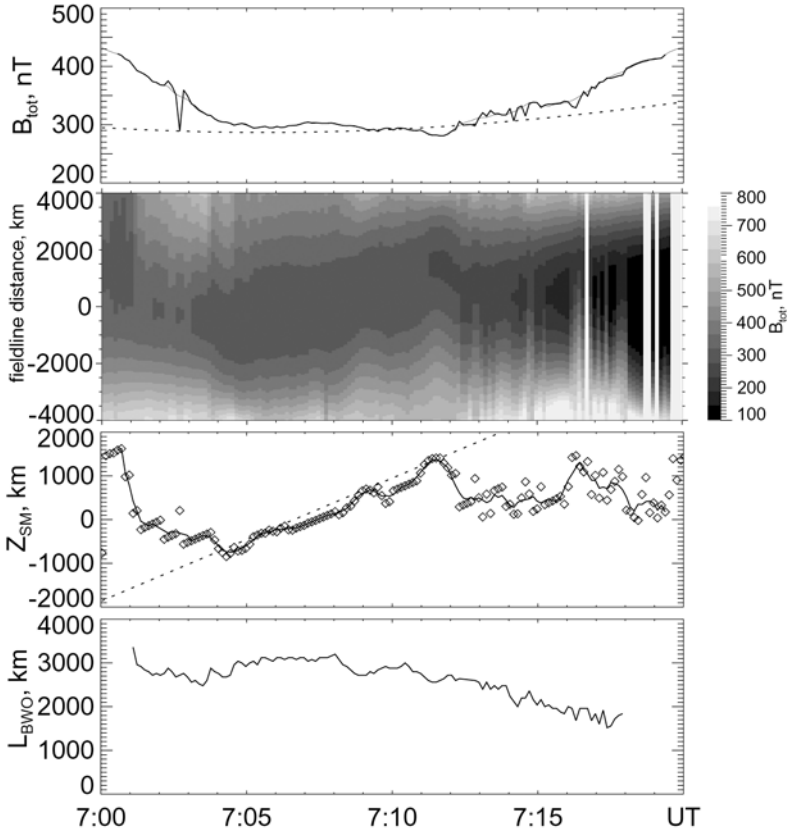

Figure 5. Same as in Figure 2 but for the event of 31 March 2001.

[21] The estimated BWO length L_{BWO} changes rather sharply during the interval of 0705–0712 UT on 31 March 2001, see Figure 5. Since L_{BWO} enters the threshold electron flux S_{thr} for the BWO instability, it is a crucial parameter determining the BWO regime. Therefore, variations in L_{BWO} should lead to the changes of the BWO generation characteristics. According to *Trakhtengerts et al.* [2004], S_{thr} can be estimated as

$$S_{\mathrm{thr}} = (N v_{\mathrm{res}})_{\mathrm{thr}} \approx \frac{m_e c^2 v_{\mathrm{res}}}{e^2\, h_{\mathrm{step}}\, L_{\mathrm{BWO}}^2} \frac{v_{\mathrm{rez}}^2}{v^2}, \tag{5}$$

where N is the number density of the energetic electrons and

$$v_{\mathrm{rez}} = \frac{\omega_{\mathrm{HL}} - \omega}{k_{\|}} = \frac{c\omega_{\mathrm{HL}}(1-\omega/\omega_{\mathrm{HL}})^{3/2}}{\omega_{\mathrm{pe}}\sqrt{\omega/\omega_{\mathrm{HL}}}} \tag{6}$$

is the parallel velocity of the resonant electrons. Here $\omega_{\mathrm{pe}} \approx 5.64 \times 10^4\, N_e^{1/2}$ is the electron plasma frequency, N_e is the cold plasma density (for this event $N_e = 5\ \mathrm{cm}^{-3}$), h_{step} is the relative height of the step on the distribution function of electrons in parallel velocities, and ω is the lowest frequency of the chorus elements. Further we assume for estimates that chorus is generated by electrons with $v_{\perp} \approx v_{\mathrm{rez}}$ and that $h_{\mathrm{step}} \approx 0.1$. When deriving equation (5) it was also assumed that $v_{\mathrm{res}} \approx v_{\|0}$, where $v_{\|0}$ is the characteristic parallel velocity of the electron distribution function.

[22] Three time intervals with different values of the S_{thr} parameter have been selected, see Figure 9. The average

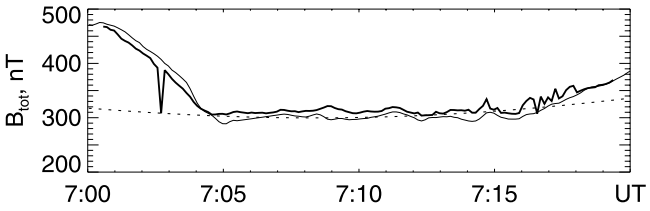

Figure 6. Same as the first panel of Figure 5 but for the Cluster 3 position.

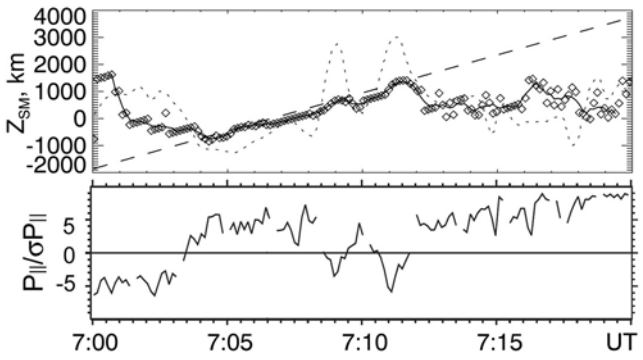

Figure 7. (top) Solid line and symbols are the position of the BWO center (minimum B point) estimated from the dynamical model of the local magnetic field, short dashed line is the position of the VLF source from *Santolik et al.* [2005], and long dashed lines are the Cluster 1 trajectory. (bottom) Parallel component of the Poynting vector normalized by its standard deviation for Cluster 1 [*Santolik et al.*, 2005].

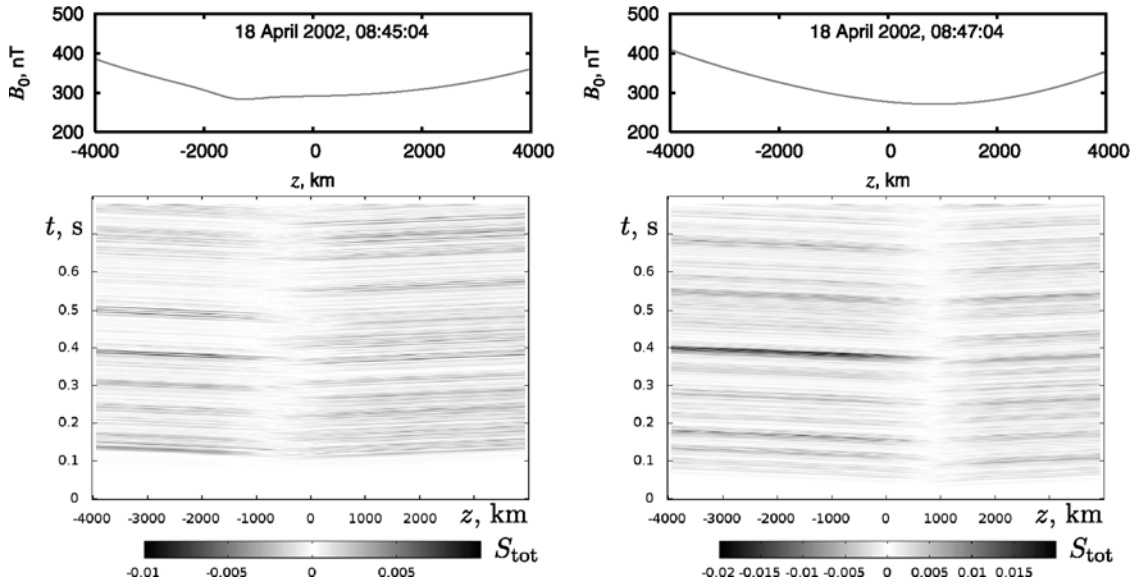

Figure 8. Results of simulations of nonlinear equations for the magnetospheric BWO [*Demekhov and Trakhtengerts*, 2005] with two magnetic field profiles corresponding to different time intervals of 18 April 2002. (top) The geomagnetic field dependences and (bottom) total Poynting flux in arbitrary units as a function of time and z coordinate. In Figure 8 bottom, the center of the source region corresponds to $S_{tot} = 0$. Note that the source center does not exactly correspond to the minimum B point, but rather forms a small region in the vicinity of this point.

number of chorus elements (at frequencies below $\omega_H/2$) and the average power (amplitude per minute) of chorus, as observed by the WBD instrument onboard Cluster [*Gurnett et al.*, 2001] are presented in Table 1 for these time intervals. One can see that these values are decreasing with an increase in the threshold flux S_{thr}. The threshold flux increases to ~30% only, while the chorus occurrence number falls by a factor ~4. This sensitivity of the chorus generation on the threshold flux can be explained by specific regime of discrete elements generation. *Kozelov et al.* [2003] presented evidence that the magnetospheric BWO operates in the so-called "on-off" intermittency regime. For this regime the average time interval between the generation peaks should be inversely proportional to the excess of the generation threshold. Taking into account this relation and the chorus characteristics from Table 1,

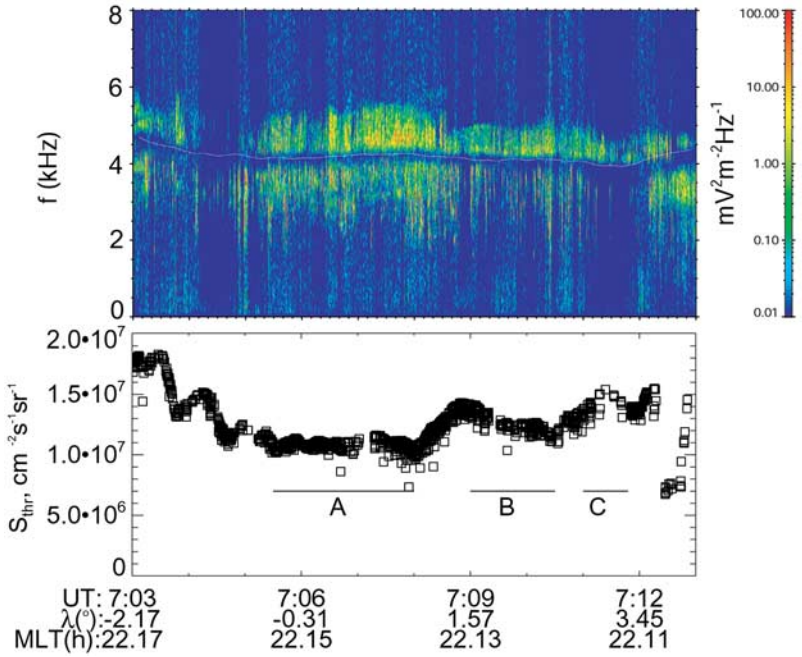

Figure 9. Cluster 1 observations on 31 March 2001. (top) Power spectrogram of the electric field. (bottom) Symbols are the estimated threshold flux ($cm^{-2}s^{-1}sr^{-1}$) for the BWO generation. Three time intervals are marked by solid lines A, B, and C.

Table 1. Chorus Characteristics in Three Intervals of Cluster 1 Observations[a]

	A	B	C
Interval (UT)	0705:30–0708:00	0709:00–0710:30	0711:00–0711:48
Average S_{thr} ($cm^{-2}s^{-1}sr^{-1}$)	1.1×10^7	1.25×10^7	1.4×10^7
Average chorus power (mV m^{-1} min^{-1})	36.4	17	5.6
Average number of elements per minute	197	141	44

[a]See Figure 9.

it is possible to estimate the flux of resonant particles. This estimates yield $S \sim 1.5 \times 10^7$ $cm^{-2}s^{-1}sr^{-1}$. This value agrees well with the integral flux $(1.3–2.3) \times 10^7$ $cm^{-2}s^{-1}sr^{-1}$ of electrons with $E > 30$ keV observed by the Research with Adaptive Particle Imaging Detectors (RAPID) onboard Cluster during the considered interval. The energy of resonant electrons should be 30–50 keV, according to the measured cold plasma density, electron gyrofrequency and lower frequency of chorus elements. More detailed analysis of particles flux data will be addressed in future works.

6. Conclusions

[23] The magnetic field data from the Cluster spacecraft are matched to a parameterized model of the local magnetic field, and the spatiotemporal dynamics of the magnetic field are obtained on this basis.

[24] The derived position of the minimum of the magnetic field at the magnetic field line passing through the spacecraft position during events of interest was found to vary substantially. These variations correspond qualitatively to the motion of the central position of the chorus source region derived previously from multicomponent measurements [*Santolik et al.*, 2005].

[25] The length and threshold flux (L_{BWO}, S_{thr}) of the magnetospheric chorus source according to the BWO model are estimated during the events of interest. The quantitative agreement between the data and the model is demonstrated by correlation of the statistical chorus characteristics with the deduced BWO parameters.

Appendix A

[26] Here we present a short description of the technique used for calculation of parameters of the additional currents from equations (1)–(3). The corresponding vectors are shown in Figure A1. The point $\mathbf{r}_1$ ($\mathbf{r}_2$) were selected according to equation (3) as a cross point of line of current I_1 (I_2) and the line $y = kx$, where k is defined by ratio from equation (3).

[27] From equation (2) we have three equations for components of vector $\mathbf{b}_1 = 2\pi\ \Delta\mathbf{B}_1/\mu_0$

$$b_{1x} = \frac{I_1 i_{1y}(p_{1z} - z_1)}{(p_{1z} - z_1)^2 + \left[i_{1x}(p_{1y} - kr_{1x}) - i_{1y}(p_{1x} - r_{1x})\right]^2} + \frac{I_2 i_{2y}(p_{1z} - z_2)}{(p_{1z} - z_2)^2 + \left[i_{2x}(p_{1y} - kr_{2x}) - i_{2y}(p_{1x} - r_{2x})\right]^2}, \quad \text{(A1)}$$

$$b_{1y} = \frac{-I_1 i_{1x}(p_{1z} - z_1)}{(p_{1z} - z_1)^2 + \left[i_{1x}(p_{1y} - kr_{1x}) - i_{1y}(p_{1x} - r_{1x})\right]^2} - \frac{I_2 i_{2x}(p_{1z} - z_2)}{(p_{1z} - z_2)^2 + \left[i_{2x}(p_{1y} - kr_{2x}) - i_{2y}(p_{1x} - r_{2x})\right]^2}, \quad \text{(A2)}$$

$$b_{1z} = \frac{I_1\left[i_{1x}(p_{1y} - kr_{1x}) - i_{1y}(p_{1x} - r_{1x})\right]}{(p_{1z} - z_1)^2 + \left[i_{1x}(p_{1y} - kr_{1x}) - i_{1y}(p_{1x} - r_{1x})\right]^2} + \frac{I_2\left[i_{2x}(p_{1y} - kr_{2x}) - i_{2y}(p_{1x} - r_{2x})\right]}{(p_{1z} - z_2)^2 + \left[i_{2x}(p_{1y} - kr_{2x}) - i_{2y}(p_{1x} - r_{2x})\right]^2}. \quad \text{(A3)}$$

[28] Similar expressions can be written for the components of $\mathbf{b}_2 = 2\pi\ \Delta\mathbf{B}_2/\mu_0$ if replacing $\mathbf{p}_1 = (p_{1x}, p_{1x}, p_{1z})$ by $\mathbf{p}_2 = (p_{2x}, p_{2x}, p_{2z})$ in equations (A1)–(A3)

$$b_{2x} = \frac{I_1 i_{1y}(p_{2z} - z_1)}{(p_{2z} - z_1)^2 + \left[i_{1x}(p_{2y} - kr_{1x}) - i_{1y}(p_{2x} - r_{1x})\right]^2} + \frac{I_2 i_{2y}(p_{2z} - z_2)}{(p_{2z} - z_2)^2 + \left[i_{2x}(p_{2y} - kr_{2x}) - i_{2y}(p_{2x} - r_{2x})\right]^2}, \quad \text{(A4)}$$

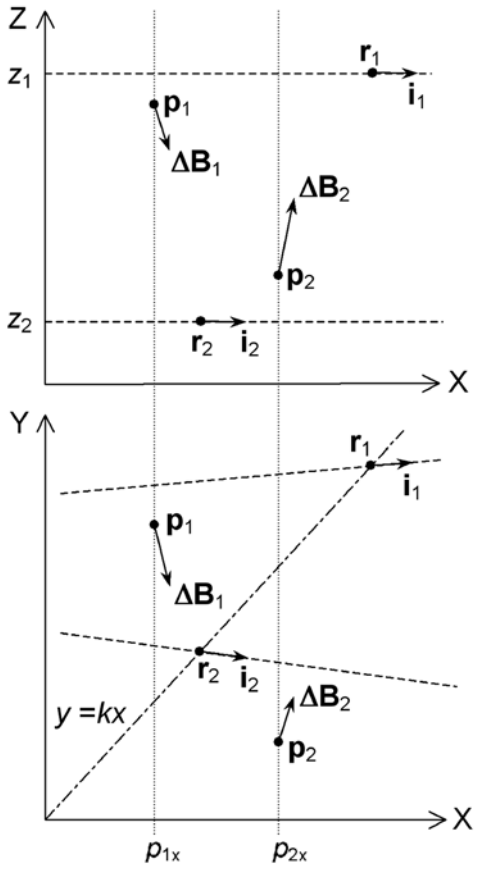

Figure A1. Schema of vectors used to fit the additional currents: $\mathbf{p}_1$ and $\mathbf{p}_2$ are positions of two Cluster satellites, $\Delta\mathbf{B}_1$ and $\Delta\mathbf{B}_2$ are deviations of the magnetic field according to equation (1), $\mathbf{r}_1$ and $\mathbf{r}_2$ are points at the line currents selected according to equation (3) at the line $y = kx$ (dashed-dotted line), dashed lines are two line currents, and i_1 and i_2 are unit vectors along their directions.

$$b_{2y} = \frac{-I_1 i_{1x}(p_{2z} - z_1)}{(p_{2z} - z_1)^2 + \left[i_{1x}(p_{2y} - kr_{1x}) - i_{1y}(p_{2x} - r_{1x})\right]^2} - \frac{I_2 i_{2x}(p_{2z} - z_2)}{(p_{2z} - z_2)^2 + \left[i_{2x}(p_{2y} - kr_{2x}) - i_{2y}(p_{2x} - r_{2x})\right]^2}, \quad \text{(A5)}$$

$$b_{2z} = \frac{I_1\left[i_{1x}(p_{2y} - kr_{1x}) - i_{1y}(p_{2x} - r_{1x})\right]}{(p_{2z} - z_1)^2 + \left[i_{1x}(p_{2y} - kr_{1x}) - i_{1y}(p_{2x} - r_{1x})\right]^2} + \frac{I_2\left[i_{2x}(p_{2y} - kr_{2x}) - i_{2y}(p_{2x} - r_{2x})\right]}{(p_{2z} - z_2)^2 + \left[i_{2x}(p_{2y} - kr_{2x}) - i_{2y}(p_{2x} - r_{2x})\right]^2}. \quad \text{(A6)}$$

By summing up (A1) and (A2) multiplied by i_{2x} and i_{2y}, respectively, we have

$$b_{1x}i_{2x} + b_{1y}i_{2y} = \frac{I_1(p_{1z} - z_1)(i_{1y}i_{2x} + i_{1x}i_{2y})}{(p_{1z} - z_1)^2 + \left[i_{1x}(p_{1y} - kr_{1x}) - i_{1y}(p_{1x} - r_{1x})\right]^2}. \quad \text{(A7)}$$

Then, we can express I_1 as

$$I_1 = \frac{(b_{1x}i_{2x} + b_{1y}i_{2y})\left\{(p_{1z} - z_1)^2 + \left[i_{1x}(p_{1y} - kr_{1x}) - i_{1y}(p_{1x} - r_{1x})\right]^2\right\}}{(p_{1z} - z_1)(i_{1y}i_{2x} + i_{1x}i_{2y})}. \quad \text{(A8)}$$

Another expression for I_1 can be found in the same way from (A4) and (A5)

$$I_1 = \frac{(b_{2x}i_{2x} + b_{2y}i_{2y})\left\{(p_{2z} - z_1)^2 + \left[i_{1x}(p_{2y} - kr_{1x}) - i_{1y}(p_{2x} - r_{1x})\right]^2\right\}}{(p_{2z} - z_1)(i_{1y}i_{2x} + i_{1x}i_{2y})}. \quad \text{(A9)}$$

Equations (A8) and (A9) allow us to exclude I_1 and obtain the relation

$$\frac{(p_{1z} - z_1)^2 + \left[i_{1x}(p_{1y} - kr_{1x}) - i_{1y}(p_{1x} - r_{1x})\right]^2}{(p_{1z} - z_1)(b_{2x}i_{2x} + b_{2y}i_{2y})} = \frac{(p_{2z} - z_1)^2 + \left[i_{1x}(p_{2y} - kr_{1x}) - i_{1y}(p_{2x} - r_{1x})\right]^2}{(p_{2z} - z_1)(b_{1x}i_{2x} + b_{1y}i_{2y})}, \quad \text{(A10)}$$

which lead to the quadratic equation for r_{1x}

$$a_1\left[i_{1x}(p_{1y} - kr_{1x}) - i_{1y}(p_{1x} - r_{1x})\right]^2 + c_1 = a_2\left[i_{1x}(p_{2y} - kr_{1x}) - i_{1y}(p_{2x} - r_{1x})\right]^2 + c_2. \quad \text{(A11)}$$

Here

$$a_1 = \left[(p_{1z} - z_1)(b_{2x}i_{2x} + b_{2y}i_{2y})\right]^{-1}, \quad c_1 = (p_{1z} - z_1)/(b_{2x}i_{2x} + b_{2y}i_{2y}),$$

$$a_2 = \left[(p_{2z} - z_1)(b_{1x}i_{2x} + b_{1y}i_{2y})\right]^{-1}, \quad c_2 = (p_{2z} - z_1)/(b_{1x}i_{2x} + b_{1y}i_{2y}).$$

[29] The expression for roots of this equation contains only two unknown variables i_{1x} and i_{2x}, since the pairs (i_{1x}, i_{1y}) and (i_{2x}, i_{2y}) are components of units vectors $\mathbf{i}_1$ and $\mathbf{i}_2$. We selected the root of this quadratic equation which corresponded to the smaller distance from the additional currents to the region of interest.

[30] A similar method was used to obtain expressions for I_2 from pairs of equations (A1), (A2), (A4), and (A5). These expressions lead to a square equation for variable r_{2x}. The roots of this equation give us the expression for r_{2x} as a function of variables i_{1x} and i_{2x}.

[31] Substitution of expressions for I_1, I_2, r_{1x}, and r_{2x} to the right-hand side of equations (A3) and (A6) leads to the system of two equations for two independent variables i_{1x} and i_{2x}. This system was solved numerically after substitution of the parameter values for each time moment. The solution yields the i_{1x} and i_{2x} values minimizing the difference between the right-hand and left-hand sides in equations (A3) and (A6). The quality of the fitting procedure was additionally tested by analyzing the difference between the calculated and measured magnetic field values. Usually this difference was less than 2 nT, as it is shown in Figures 2 and 5.

[32] **Acknowledgments.** We acknowledge the access to the spin resolution data of the FGM magnetic field experiment (provided by A. Balogh and E. Lucek). We thank R. Huff, J. Dowell, J. Seeberger, and other colleagues from the University of Iowa for the calibration and preprocessing of the WBD measurements. This study was supported by INTAS (grant 03-51-4132) and EU LAPBIAT program (RITA-CT-2006-025969). The work of E.E.T., B.V.K., A.G.D., and V.Y.T. was supported by the Russian Foundation for Basic Research (grants 04-05-64955 and 05-02-16459) and by the Russian Academy of Sciences through the basic research program "Solar Activity and Physical Processes in the Sun-Earth System." The WBD measurements were supported by the NASA Goddard Space Flight Center under grants NAG5–9974 and NNG04GB98G. O.S. and E.M. acknowledge additional support from the NSF award 0307319/KONTAKT ME 842 and GAAV grant IAA 301120601. This paper is dedicated to Victor Trakhtengerts, our dear friend and colleague, the head, soul and heart of our collaboration.

[33] Wolfgang Baumjohann thanks the reviewers for their assistance in evaluating this paper.

References

Baker, D. N., R. E. Ergun, J. L. Burch, J. M. Jahn, P. W. Daly, R. Friedel, G. D. Reeves, T. A. Fritz, and D. G. Mitchell (2002), A telescopic and microscopic view of a magnetospheric substorm on 31 March 2001, *Geophys. Res. Lett.*, *28*(18), 1862, doi:10.1029/2001GL014491.

Balogh, A., et al. (2001), The Cluster magnetic field investigation: Overview of in-flight performance and initial results, *Ann. Geophys.*, *19*, 1207–1217.

Demekhov, A. G., and V. Y. Trakhtengerts (2005), Dynamics of the magnetospheric cyclotron ELF/VLF maser in the backward-wave-oscillator regime. part I: Basic equations and results in the case of a uniform magnetic field, *Radiophys. Quantum Electron.*, *48*(9), 639–649, doi:10.1007/s11141-005-0109-3.

Demekhov, A. G., D. Nunn, and V. Y. Trakhtengerts (2003), Backward wave oscillator regime of the whistler cyclotron instability in an inhomogeneous magnetic field, *Phys. Plasmas*, *10*(11), 4472–4477, doi:10.1063/1.1620507.

Gurnett, D. A., et al. (2001), First results from the Cluster wideband plasma wave investigation, *Ann. Geophys.*, *19*, 1259–1272.

Kozelov, B. V., and T. V. Kozelova (2003), Dynamics of domains of non-adiabatic particle motion in the near magnetosphere during a substorm, *Geomagn. Aeron. Engl. Transl.*, *43*(4), 488–497.

Kozelov, B. V., E. E. Titova, A. A. Lyubchich, V. Y. Trakhtengerts, and Y. Manninen (2003), On-off intermittency as a possible mechanism of formation of ELF-VLF chorus series, *Geomagn. Aeron. Engl. Transl.*, *43*(5), 593–601.

LeDocq, M. J., D. A. Gurnett, and G. B. Hospodarsky (1998), Chorus source locations from VLF Poynting flux measurements with the Polar spacecraft, *Geophys. Res. Lett.*, *25*(21), 4063–4066, doi:10.1029/1998GL900071.

Santolik, O., and D. A. Gurnett (2003), Transverse dimensions of chorus in the source region, *Geophys. Res. Lett.*, *30*(2), 1031, doi:10.1029/2002GL016178.

Santolík, O., D. A. Gurnett, J. S. Pickett, M. Parrot, and N. Cornilleau-Wehrlin (2004), A microscopic and nanoscopic view of storm-time chorus in 31 March 2001, *Geophys. Res. Lett.*, *31*, L02801, doi:10.1029/2003GL018757.

Santolik, O., D. A. Gurnett, J. S. Pickett, M. Parrot, and N. Cornilleau-Wehrlin (2005), Central position of the source region of storm-time chorus, *Planet. Space Sci.*, *53*, 299–305, doi:10.1016/j.pss.2004.09.056.

Trakhtengerts, V. Y. (1995), Magnetosphere cyclotron maser: Backward wave oscillator generation regime, *J. Geophys. Res.*, *100*(A9), 17,205–17,210, doi:10.1029/95JA00843.

Trakhtengerts, V. Y. (1999), A generation mechanism for chorus emission, *Ann. Geophys.*, *17*, 95–100, doi:10.1007/s005850050739.

Trakhtengerts, V. Y., A. G. Demekhov, E. E. Titova, B. V. Kozelov, O. Santolik, D. Gurnett, and M. Parrot (2004), Interpretation of Cluster data on chorus emissions using the backward wave oscillator model, *Phys. Plasmas*, *11*(4), 1345–1351, doi:10.1063/1.1667495.

Tsyganenko, N. A., and M. I. Sitnov (2005), Modeling the dynamics of the inner magnetosphere during strong geomagnetic storms, *J. Geophys. Res.*, *110*, A03208, doi:10.1029/2004JA010798.

Tsyganenko, N. A., and D. P. Stern (1996), A new-generation global magnetosphere field model, based on spacecraft magnetometer data, *Int. Sol. Terr. Phys. Program Newsl.*, *6*(1), 21.

A. G. Demekhov, Institute of Applied Physics, 46 Ulyanov Street, 603950 Nizhny Novgorod, Russia.

D. A. Gurnett and J. S. Pickett, Department of Physics and Astronomy, University of Iowa, 203 Van Allen Hall, Iowa City, IA 52242, USA.

B. V. Kozelov, Department of Physics and Technology, University of Tromsø, Prestvannveien 40, N-9011 Tromsø, Norway. (boris.kozelov@gmail.com)

E. Macusova, Department of Mathematics and Physics, Charles University, Celetná 13, 116 36 Prague 1, Czech Republic.

O. Santolik, Institute of Atmospheric Physics, Boèní II 1401, 141 31 Prague 4, Czech Republic.

E. E. Titova, Polar Geophysical Institute, Fersman Street 14, Apatity, 184209 Russia.